Structural and electronic properties of single-walled AlN nanotubes of different chiralities and sizes

2006 J. Phys.: Condens. Matter 18 S2045

(http://iopscience.iop.org/0953-8984/18/33/S20)

INSTITUTE OF PHYSICS PUBLISHING JOURNAL OF PHYSICS: CONDENSED MATTER

J. Phys.: Condens. Matter **18** (2006) S2045–S2054 doi:10.1088/0953-8984/18/33/S20

Structural and electronic properties of single-walled AlN nanotubes of different chiralities and sizes

Yu F Zhukovskii[1,5], A I Popov[1,2], C Balasubramanian[3,4] and S Bellucci[3]

[1] Institute for Solid State Physics, University of Latvia, Kengaraga 8, Riga LV-1063, Latvia
[2] Institut Laue-Langevin, 6 rue Jules Horowitz, 38042 Grenoble, France
[3] INFN-Laboratori Nazionali di Frascati, Via Enrico Fermi 40, I-00044 Frascati, Italy
[4] Department of Environmental, Occupational and Social Medicine, University of Rome Tor Vergata, Via Montpellier 1, I-00133 Rome, Italy

E-mail: quantzh@latnet.lv

Received 31 January 2006
Published 4 August 2006
Online at stacks.iop.org/JPhysCM/18/S2045

Abstract

Four models of single-walled AlN nanotubes (NTs), which possess (i) two different chiralities (armchair or zigzag type) and (ii) two different uniform diameters for both types of NTs (1 or 6 nm) have been constructed, in order to analyse the dependence of their properties on both morphology and thickness. Periodic one-dimensional (1D) DFT calculations performed on these models have allowed us to analyse how the chirality and curvature of the NT change its properties as compared to both AlN bulk with either wurtzite or zinc-blende structures and their densely packed surfaces. We have found that the larger the diameter of the AlN NT, the smaller the width of its bandgap, the strengths of its bonds and the charge separations in them. This confirms the recent experimental finding of the possibility to adjust electronic properties in ultimate nanoscale optoelectronic devices produced from AlN and other group III nitrides.

(Some figures in this article are in colour only in the electronic version)

1. Introduction

Among the group III nitrides, AlN is the largest bandgap semiconductor ($\Delta\varepsilon_g$ reaches 6.2 eV), which is characterized by high temperature stability, considerable thermal conductivity, low thermal expansion, resistance to chemicals and gases used in semiconductor processing and reliable dielectric properties [1–3]. Moreover, the small lattice mismatch between AlN, GaN and InN makes possible a synthesis of heterostructural alloy systems. For instance, since $\Delta\varepsilon_g$ for the two latter nitrides is 3.4 and 1.9 eV, respectively, $In_xAl_{1-x}N$ and $In_yGa_{1-y}N$ have been recently used for bandgap engineering by controlling the indium composition [4]. This is why these materials are widely used in a number of technological applications, mainly in micro- and

[5] Author to whom any correspondence should be addressed.

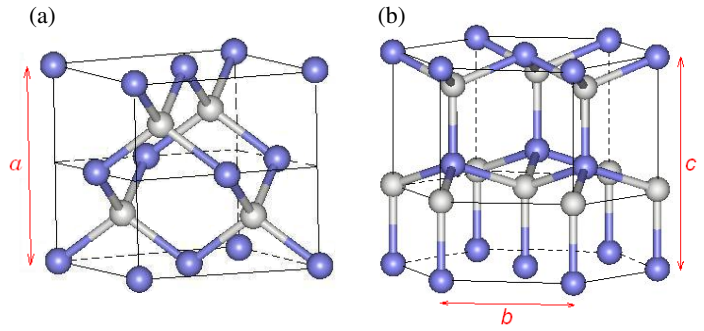

Figure 1. Images and lattice parameters of unit cells for the two AlN phases: (a) zinc-blende ($F\bar{4}3m$ space group) and (b) wurtzite ($P6_3mc$ space group). Parameters of both AlN lattices were first obtained experimentally ($a = 4.38$ Å, $b = 3.11$ Å and $c = 4.98$ Å [1]) and then confirmed theoretically. Light grey balls correspond to Al atoms and N atoms are shown by dark grey (blue).

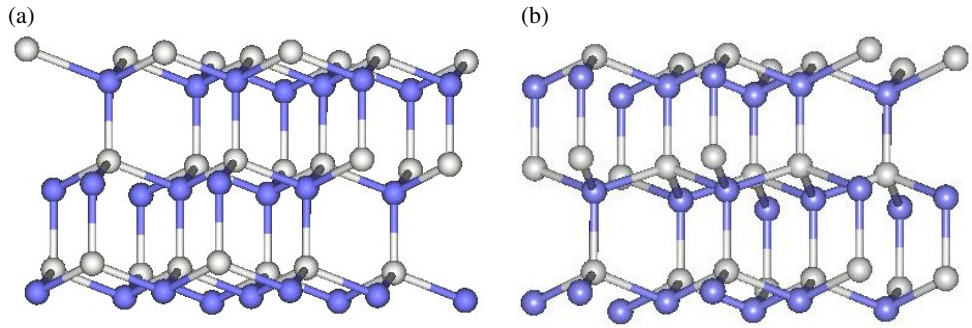

Figure 2. Images of the densely packed six-layer slabs n-type-terminated from both sides for both AlN phases: (a) zinc-blende(111) diamond-like surface and (b) wurtzite(0001) surface. For graphical details, see explanations given in figure 1.

optoelectronics, for instance laser diodes and 'solar-blind' ultraviolet photodetectors [3]. Their performance can be noticeably improved by the regulation of extrinsic impurities and intrinsic point defects inside the crystalline samples [5].

There are three possible three-dimensional (3D) crystal morphologies shared by the group III nitrides: the wurtzite (w-), zinc-blende (zb-) and rock-salt (rs-) structures [6]. Aluminium nitride usually crystallizes in the hexagonal (w-AlN) structure (figure 1(b)), which is described by the $P6_3mc$ space group. As to the zb-structure ($F\bar{4}3m$ group) shown in figure 1(a), it was found to be metastable in AlN, although for GaN and InN it can be stabilized using epitaxial growth of their thin films on the (001) planes of face-centred cubic structures like MgO [7]. The rs-structure ($Fm\bar{3}m$ group) in the group III nitrides can be achieved at very high pressures only, thus it is not usually considered. Such a structural polytypism is rather typical for wide bandgap semiconductors. Numerous theoretical studies of w-AlN and zb-AlN phases [1–8] clearly show that the latter is characterized by noticeably smaller bandgap (this difference reaches several tenths of an eV). Moreover, both phases differ from each other in the stacking sequence along the [0001] direction in the wurtzite structure and [111] in the zinc-blende one [9], which cross the most densely packed crystallographic faces of AlN and other group III nitrides.

2D plane structures of the group III nitrides have been studied mainly for the densely packed polar surfaces of wurtzite (0001) (figure 2(b)) and zinc-blende (111) (figure 2(a)).

A common feature found for all polar surfaces is a strong tendency towards a metal-rich surface stoichiometry whereas nitrogen ions are rather thermodynamically unstable on almost all equilibrium surfaces [10, 11]. Recent studies demonstrated that in w-structures two kinds of surfaces are most stable: (i) the so-called n-type, or (0001) surface, where the first interlayer is honeycomb as shown in figure 2(a); (ii) the p-type, or $(000\bar{1})$ surface, where the outer metal atoms are positioned directly above the subsurface nitrogen atoms. The n-type surfaces usually exhibit a smoother surface morphology, leading to a higher material quality [10]. Moreover, if the n-type surface of the group III nitrides is characterized by a bandgap which is 2–2.5 times more narrow than that in bulk, then the p-type surface possesses practically no noticeable gap between the conduction band and valence band since it is completely overlapped by energy states of outer metal layer which is bound with subsurface layers weaker than that in the case of n-type substrate. Analogously, the n-type (111) surface (figure 2(b)) is the most favourable for the zinc-blende polar substrate. Unlike other group III nitrides, BN can also exist in the so-called graphitic hexagonal form where the nearest boron and nitrogen ions are positioned within the one surface layer [12].

Beginning with the discovery of carbon multi-walled nanotubes with unique properties [13] considerable efforts were undertaken to synthesize 1D periodic nanostructures, such as nanotubes (NTs) and nanowires (NWs), from other inorganic materials [14, 15]. Among these materials, group III nitride nanostructures attract enhanced attention of both experimentalists and theorists [15–19], due to numerous technological applications, for instance AlN in GaN-based nanoelectronics [20] AlN NTs were recently synthesized experimentally using either direct current (DC) arc-plasma-induced melting of aluminium in N–Ar ambient [16] or treating the aluminium powder, impregnated with cobalt sulfate in advance, with NH_3/N_2 in a special tubular furnace [17]. In both cases nanotube samples identified using high-resolution transmission electron microscopy (HRTEM) were accompanied by nanoparticles and nanowires. Actually, experimentally observed NTs are rather smooth nano-rods with hollow centres and comparatively thick walls which are characterized by Al and N arranged in hexagonal crystalline structure, similar to bulk w-AlN [18]. Diameters of these nanotubes were found to be either small, 2–4 nm, or large, 20–80 nm, whereas the thicknesses of their walls were estimated to be from 1 up to 20 nm. Unlike synthesized boron nitride NTs, which were recently observed with graphitic and honeycomb network on the tube wall [20], no experimental observation of such single-walled structures in AlN, GaN and InN has been reported so far. Probably this difference can be due to the existence of graphitic and honeycomb sheet structures observed in the BN surface as mentioned above (which can be rolled up in single-walled NTs) whereas in other group III nitrides they cannot exist.

Nevertheless, almost all theoretical simulations on the group III nitride NTs performed so far have used just the smooth single-walled model [18, 19, 21–27] as the simplest presentation of the 1D nanostructures. They are characterized by two equilibrium structures possessing either armchair- or zigzag-type chiralities (figure 3) and a wide range of uniform diameters (0.5–2 nm). Due to sp^2 hybridization of metal–nitrogen bonds, these graphite-like layered tubular structures were found to be energetically stable. For theoretical simulations on these models, both finite cage-like clusters [18, 19, 21] and 1D nanotubes [22–27] were used. A wide spectrum of methods was applied in these calculations: atomistic formalism of many-body empirical potentials [27] as well as first principles Hartree–Fock (HF) and density functional theory (DFT) methods realized in the framework of localized atomic functions or plane waves [18, 19, 21–26]. Several interesting results were obtained in these studies: (i) zigzag NTs possess a direct bandgap, which means that such nanostructures may exhibit strong electro-luminescence never observed in their bulk materials [8], whereas armchair NTs have

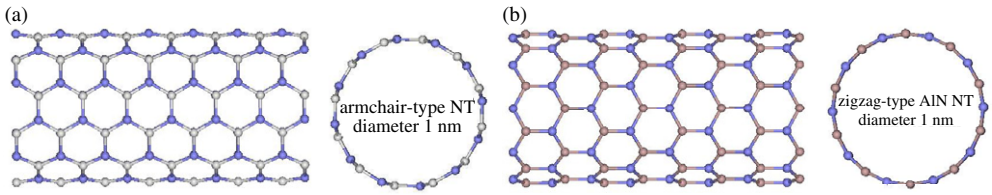

Figure 3. Images of 1 nm thick AlN NTs along the axes of nanotubes and across them for (a) armchair-type and (b) zigzag-type chiralities. For graphical details, see the explanations given in figure 1. For better distinction between both chiralities, Al atoms for the latter type are shown in medium grey (brown).

an indirect bandgap; (ii) these bandgaps still remain wide enough to keep semiconductor properties of NTs although they are less by 0.5–1.5 eV than those in bulk materials; (iii) with increasing NT diameter the change of the bandgap width is still not clear: according to cluster (cage-like) models it reduces [21] whereas plane wave calculations lead to a slight increase [23, 26]; (iv) in cage-like models, the binding energy was about 9–11 eV per AlN pair [21, 22]; (v) using the force-field conjugate gradient algorithm combined with the first principle calculations [24], the thermal stability of the AlN NTs was simulated: it was shown that single-walled nanotubes can stably exist at room temperature ($T \sim 300$ K) and melt at $T > 600$ K. Thus, experimental synthesis of AlN and other group III nitrides (except for BN) nanotubes with ultrathin wall would be highly appreciated.

In this study, we perform DFT calculations on structural and electronic properties of (i) AlN bulk (both wurtzite and zinc-blende) (figure 1), (ii) polar n-type w-AlN(0001) and zb-Al(111) surfaces (figure 2), (iii) AlN NTs with two different chiralities (armchair or zigzag type) and two different uniform diameters (1 and 6 nm) (figures 3 and 4). This should clarify a trend in the change of the electronic properties of AlN NTs depending on their morphology and size. No similar comparison has been reported so far, nor has anybody constructed so large a nanotube diameter (6 nm) when performing the first principles atomistic simulations. This can also indicate the next steps for both theoretical and experimental studies of AlN NTs to achieve the certain conformity between their results.

2. Theoretical background

Using formalism of the localized Gaussian-type functions (GTFs) as implemented in the *CRYSTAL-03* code [28] we have performed periodic DFT calculations on the two 3D models of AlN bulk (figure 1), two 2D models of the densely packed surfaces of both AlN phases (figure 2) and four 1D models of single-walled AlN nanotubes (figures 3 and 4). For these calculations, we have used the non-local PWGGA (Perdew–Wang generalized gradient approximation) exchange–correlation functional [29]. The all-valence basis sets for Al and N GTFs (8s–511sp–1d and 81s–31p–1d, respectively) were optimized elsewhere (for several Al-containing crystalline compounds [30] and group III nitrides [31]), therefore we only slightly have re-optimized their valence and virtual shells.

When performing the optimization of bulk structures shown in figure 1 we have fixed their symmetry and have changed only their optimized lattice parameters: one (a) for the cubic structure as well as two (b and c) for the hexagonal structure which should be optimized synchronously, according to the initial ratio between their lengths.

When optimizing the substrate structures shown in figure 2 we have fixed lattice parameters optimized for the corresponding bulk phases and have optimized only external interlayer

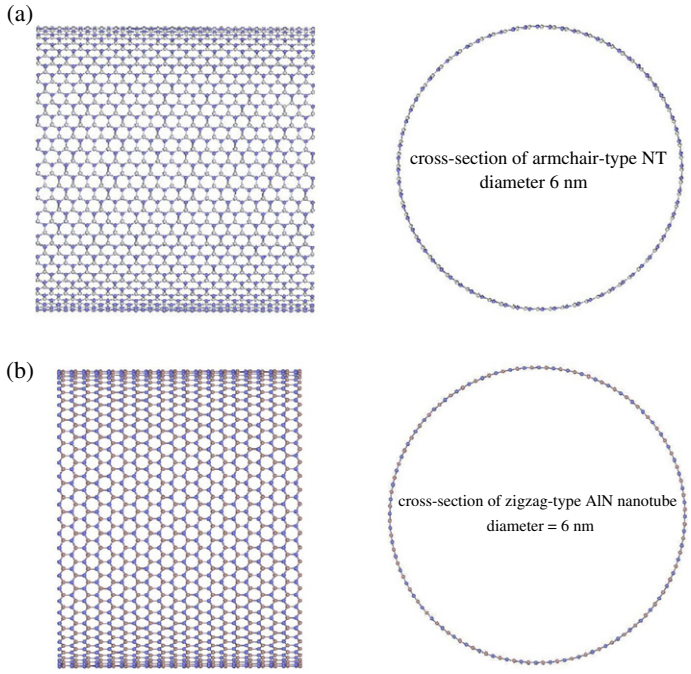

Figure 4. Images of 6 nm thick AlN NTs along the axes of nanotubes and across them for (a) armchair-type and (b) zigzag-type chiralities. For graphical details, see explanations given in figures 1 and 3.

distances from both sides of slabs cut from both bulk phases. It is well seen that atomic coordinates of the first three layers from the top Al-terminated surfaces coincide for both substrates (both images in figure 2 are mirror inverted), whereas the orientation of atoms in deeper layers differs by turning through 180° concerning the corresponding Al–N bonds normal to the surface.

Models of the 1 and 6 nm armchair-type AlN NTs have been considered as (n, n) periodic structures (rod symmetry Pn/m) which include 24 and 144 atoms in the corresponding 1D unit cells (6, 6) (figure 3(a)) and (36, 36) (figure 4(a)). For the 1 and 6 nm zigzag-type AlN NTs (rod symmetry $Pnmm$), we have constructed (10, 0) (figure 3(b)) and (64, 0) (figure 4(b)) unit cells which include 40 and 256 atoms, respectively. For all the AlN NT models, we have optimized the length of the nearest AlN bond, which results in the changes of the corresponding nanotube diameters as well.

For 3D, 2D and 1D models shown in figures 1–4, we have determined the binding energy per AlN pair and the charge transfer along it (table 1). For the former, we use the following expression:

$$E_{\mathrm{bind}}(\mathrm{Al–N}) = E_{\mathrm{tot}}(\mathrm{AlN\ molecule}) - \frac{E_{\mathrm{tot}}(\mathrm{unit\ cell\ of\ AlN\ model})}{n_{\mathrm{AlN}}}, \qquad (1)$$

where E_{tot} is the calculated total energy per molecule or unit cell and n_{AlN} a number of AlN pairs per unit cell. In order to construct the total as well as Al- and N-projected densities of states (DOSs) for all these models, we have used the reciprocal space integration with the suitable shrinking factors for the Monkhorst–Pack and Gilat nets: $4 \times 4 \times 8$ [32, 33].

Table 1. Calculated structural and electronic properties for the models of 3D, 2D and 1D AlN.

		Bulk (figure 1)		Surface (figure 2)[a]		Single-walled NT (figures 3, 4)			
Properties	Source	w-AlN	zb-AlN	w-(0001)	zb-(111)	(6, 6)	(10, 0)	(36, 36)	(64, 0)
Equilibrium bond length r_{min} (Al–N) (Å)	Our data	1.86	1.88	1.841	1.835	1.790	1.794	1.801	1.804
	Reference	1.89 [8]	1.90 [24]		—		1.77 [19], 1.83 [18]		
Binding energy per AlN pair E_{bind} (Al–N) (eV)	Our data	14.37	14.26	11.51	11.41	12.80	12.79	12.67	12.66
	Reference	16.0 [24]			—		9.0 [18], 10–11 [21]		
Effective charge q_{Al} and $\lvert q_N \rvert$, e	Our data	2.27	2.22	2.20	2.18	2.26	2.26	2.23	2.22
	Reference	—		—			2.55 [8]		
Energy gap $\Delta\varepsilon_{gap}$ (eV) (figure 5)	Our data	7.4	7.2	2.5	2.1	7.1	7.0	6.8	6.6
	Reference[b]	6.2 [8]	5.2–5.7 [1, 9]		<2 [11]		4.8–5.6 [21]		

[a] The corresponding values are averaged across the slabs.
[b] We have not included here results of several LDA calculations underestimating $\Delta\varepsilon_{gap}$ by more than 1 eV.

3. Results and discussion

In this paper, we analyse the calculated structural and electronic properties for different morphologies of aluminium nitride bulks, surfaces and nanotubes (table 1 and figures 5 and 6) as well as comparing them with available experimental and theoretical data obtained for the same materials. According to our calculations, optimized lattice constants for AlN with zinc-blende and wurtzite structures are found to be very close to the corresponding experimental data mentioned above: $a = 4.35$ (4.38) Å, $b = 3.08$ (3.11) Å and $c = 4.94$ (4.98) Å (experimental data are written in brackets). Thus, for bulk structures, we consider only the nearest Al–N distances as shown in table 1.

Results presented in table 1 show a certain difference between the properties of both phases of AlN (bulk and surface) confirmed by data available in the literature. When comparing AlN NTs of various sizes and chiralities this difference is noticeably smaller, especially for nanotubes of the same thickness. At the same time, the larger an AlN nanotube diameter, the closer E_{bind}(Al–N), q_{Al} ($|q_N|$) and $\Delta\varepsilon_{gap}$ are to the corresponding values obtained for the densely packed surfaces with hexagonal structure; at least, these values decrease. This trend is also confirmed by analysis of curving sheet-to-cylinder strain energy: it noticeably reduces with increase of NT diameter [27]. However, since we have used six-layer slab models (figure 2), presented values of E_{bind}(Al–N), q_{Al} ($|q_N|$) and $\Delta\varepsilon_{gap}$ for both surfaces are rather averaged between AlN bulk and graphitic or honeycomb single-walled slabs. Qualitatively, values presented in table 1 correspond to those obtained in various theoretical and experimental studies. For example, smaller ionicity of the Al–N bond in zb-AlN as compared to w-AlN bulk was obtained in LDA calculations [34] (the ratio of their ionicity factors is 0.44/0.46, which can be compared with the corresponding ratio of effective charges, 2.22/2.27). The ratio of covalency factors is opposite. We have obtained that 1.5–1.6 e is shared along the Al–N bond in the bulk. However, the AlN molecule is a substantially more covalent compound: $q_{Al} = +1.5\,e$ and $q_N = -1.5\,e$, according to our calculations. In any case, the maximum of the electronic density along the covalent bond is shifted towards N [34].

As to the qualitative difference of our results presented in table 1 as well as figures 5 and 6 with a slight asymptotic increase of $\Delta\varepsilon_{gap}$ for the larger AlN NTs observed in [23], it

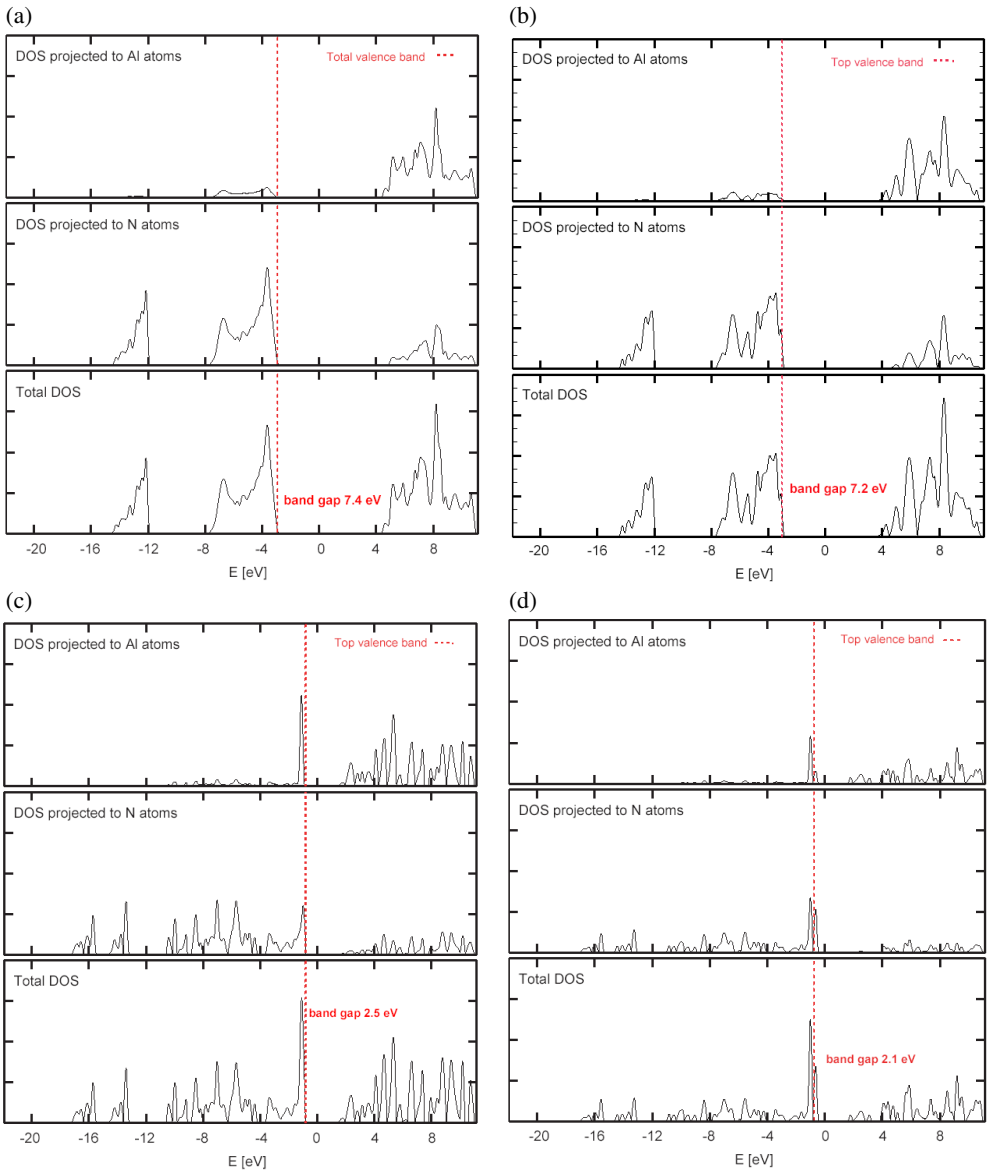

Figure 5. Total and projected densities of one-electron states (DOSs) for (a) w-AlN bulk, (b) zb-AlN bulk, (c) w-AlN(0001) surface and (d) zb-AlN(111) surface. All details of DOSs are described inside plots; moreover, values of $\Delta\varepsilon_{\mathrm{gap}}$ are presented in table 1.

could be caused by the factor that calculations in that study were performed for nanotubes with diameters up to 1.5–2.0 nm only, which are too thin to observe any approach to the surface properties. Moreover, most of the previous calculations on bandgaps performed for AlN crystals and nanotubes markedly underestimated $\Delta\varepsilon_{\mathrm{gap}}$ (including [23]). Quite on the contrary, in our calculations, the bandgap for w-AlN bulk is overestimated by ∼1.2 eV as compared to the experimental value of 6.2 eV [8]. As a result of this difference, disagreement in the description of the dependence of $\Delta\varepsilon_{\mathrm{gap}}$ on NT diameter is also possible.

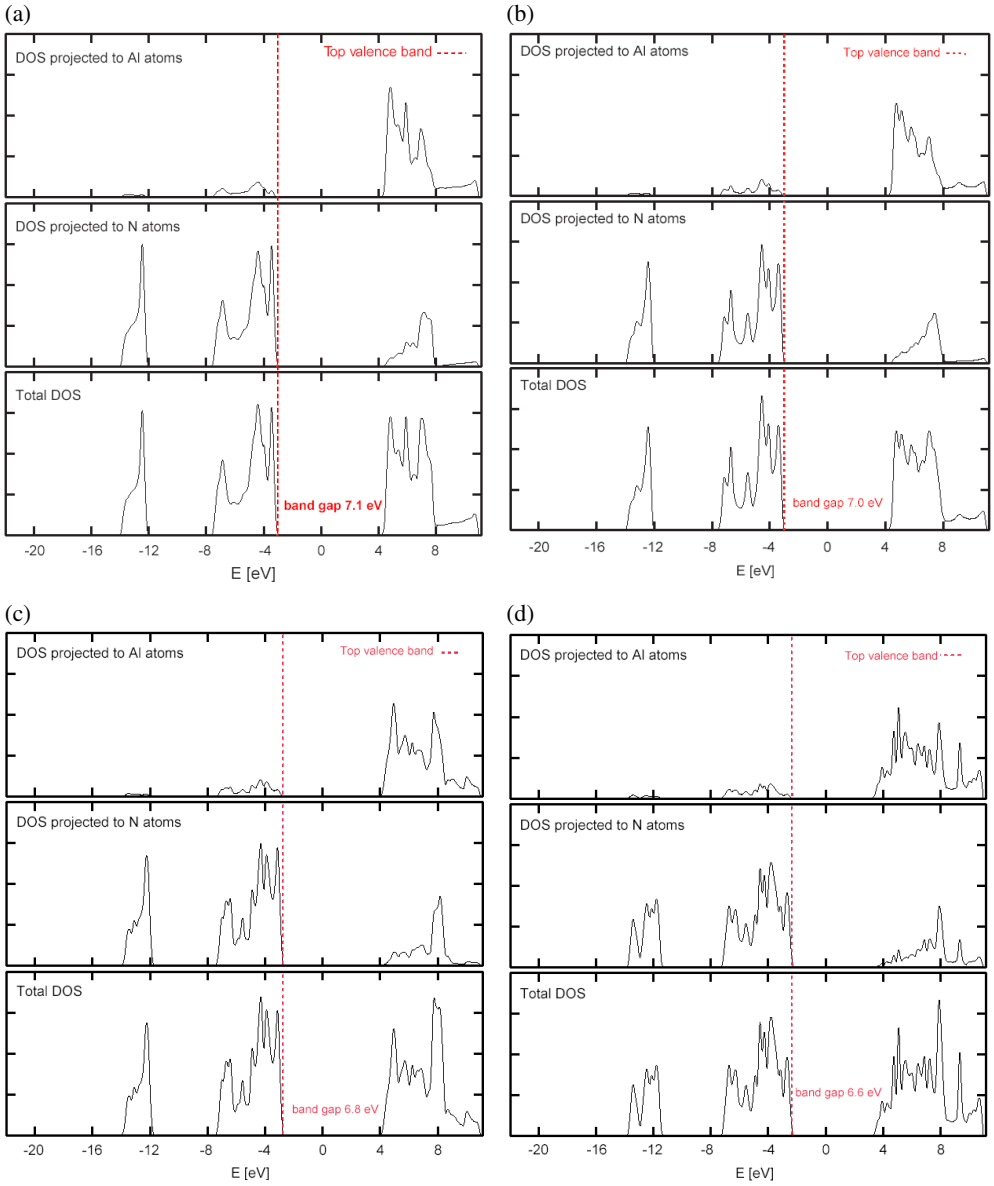

Figure 6. Total and projected densities of one-electron states (DOSs) for AlN NTs: (a) 1 nm armchair-type (6, 6) (figure 3(a)), (b) 1 nm zigzag-type (10, 0) (figure 3(b)), (c) 6 nm armchair-type (36, 36) (figure 4(a)), (d) 6 nm zigzag-type (64, 0) (figure 4(b)). For details, see explanations given in figure 5.

Detailed qualitative analysis of total and atom-projected DOS with the angular momentum decomposition for both w-AlN and zb-AlN bulk phases was performed elsewhere [34]. Analysing our DOS presented in figures 5 and 6, we can observe qualitative similarities with explanations formulated in that paper. For example, while no dramatic difference is observed between the total DOSs for both bulk phases in the area of valence bands (figures 5(a) and (b)), significant discrepancies are obvious for the unoccupied levels: the bottom of the conduction

band for zb-AlN is shifted towards lower energies as compared to that of w-AlN. For both phases, the total DOS presents three regions: the lower part of the valence bands is dominated by N(2s) states, its upper parts characterized by superposition of N(2p) and Al(3p) states, with smaller contribution of Al(3s), whereas the first conduction band is predominantly Al(3s). Thus, the strength of the Al–N bond is mainly due to the strong hybridization of Al(3s) and Al(3p) with N(2p) states. When we consider the DOS for w-(0001) and zb-(111) surfaces (figures 3(c) and (d)), their bandgap is markedly reduced as compared to AlN bulk; moreover, distribution of levels in the surface DOS is much more discrete. From this point of view, the DOS of 6 nm AlN NTs is closer to the surface DOS than that for 1 nm AlN NTs, which can be considered as an additional argument in favour of the approach of properties for nanotubes with increasing size to surface properties.

While we perform simulations on densely packed AlN surfaces, we have to achieve a reliable level of their adequate description. It has been mentioned above that the most stable surfaces of the group III nitrides possess n-type surface structure and metal termination. The first requirement has been realized in our simulations (figure 2). However, we do not consider odd-layer slab models of surfaces, metal terminated from both sides, since in such a case we can face an artificial charge re-distribution inside the slab. On the other hand, the bottom N-terminated side of the slab certainly distorts both the total and projected DOS shown in figures 5(c) and (d). Thus, we have to take into account necessary corrections for the current data, in order to represent the electronic structure of AlN surfaces more adequately.

4. Summary

In this study we have performed systematic non-local DFT (PWGGA) calculations on the smooth single-walled AlN nanotubes possessing the two different chiralities (armchair and zigzag type) and sizes (1 and 6 nm) as well as two phases of AlN bulk and their densely packed surfaces. All calculations show stability of 3D, 2D and 1D systems under study. When performing these calculations we could also analyse their structural and electronic properties as well as comparing them with available data in the literature. As a result we can show that the larger the NT diameter, the closer its electronic and structural properties to those of hexagonal AlN surfaces. Nevertheless, so far, synthesis of AlN NTs cannot lead to a formation of single-walled nanostructures [15–17]. This is why our further model of NT wall structure should be closer to a six-layer slab, which has been considered in our current simulations. At the same time we must be more accurate with an adequate simulation of AlN surfaces. Else one step in our further activity is an increase of AlN NT diameter, in order to be sure that our conclusions made in this paper do not depend on the nanotube size. Moreover, we have to achieve a closer correlation between the properties, which can be both calculated theoretically and measured experimentally, for instance, between the DOS and photoelectron spectra.

Acknowledgments

This study was supported by the TARI (Transnational Access to Research Infrastructures) program at the National Laboratory of Frascati, Italy. The authors kindly thank A Gulans and S Piskunov for technical assistance.

References

[1] Strite S and Morkoç H 1992 *J. Vac. Sci. Technol.* B **10** 1237
[2] Jain C, Willander M, Narayan J and van Overstraeten R 2000 *J. Appl. Phys.* **87** 965

[3] Ruterana P, Albrecht M and Neugebauer J 2003 *Nitride Semiconductors: Handbook on Materials and Devices* (New York: Wiley)
[4] Jenkins D W and Dow J D 1989 *Phys. Rev.* B **39** 3317
[5] Mireles F and Ulloa S E 1998 *Phys. Rev.* B **58** 3879
[6] Morkoç H 1999 *Nitride Semiconductors and Devices* (*Springer Series in Material Science* vol 32) (Berlin: Springer)
[7] Meyer B K 1998 *III V Nitrides Semiconductors and Ceramics: from Material Growth to Device Applications* (Amsterdam: Elsevier Health Sciences)
[8] Vurgaftman I and Meyer J R 2003 *J. Appl. Phys.* **94** 3675
[9] Stampfl C and Chris G 1998 *Phys. Rev.* B **57** R15052
[10] Zywietz T K, Neugebauer J and Scheffler M 1999 *Appl. Phys. Lett.* **74** 1695
[11] Wu C I and Kahn A 1999 *Appl. Phys. Lett.* **74** 546
[12] Collazo-Davila C, Bengu E, Leslie C and Marks L D 1998 *Appl. Phys. Lett.* **72** 314
[13] Iijima S 1991 *Nature* **354** 2148
[14] Davis J H 1998 *Physics of Low Dimensional Structures* (Cambridge: Cambridge University Press)
[15] Bellucci S 2005 *Phys. Status Solidi* c **2** 34
Bellucci S 2005 *CANEUS 2004-Conf. on Micro-Nano-Technologies (Nov. 2004)*; *Nucl. Instrum. Methods* B **234** 57
[16] Balasubramanian C, Godbole V P, Rohatgi V K, Das A K and Bhoraskar S 2004 *Nanotechnology* **15** 370
Balasubramanian C, Bellucci S, Castrucci P, De Crescenzi M and Bhoraskar S V 2004 *Chem. Phys. Lett.* **383** 188
[17] Wu Q, Hu Z, Wang X, Lu Y, Chen X, Xu H and Chen Y 2003 *J. Am. Chem. Soc.* **125** 10176
[18] Hou S, Zhang J, Shen Z, Zhao X and Xue Z 2005 *Physica* E **27** 45
[19] Zhang D and Zhang R Q 2003 *Chem. Phys. Lett.* **371** 426
[20] Golberg D, Bando Y, Eremets M, Takemura K, Kurashima K and Yusa H 1996 *Appl. Phys. Lett.* **69** 2045
[21] Zope R R and Dunlap B I 2005 *Phys. Rev.* B **72** 045439
[22] Lee S, Lee Y, Hwang Y, Elsner D, Porezag D and Frauenheim T 1999 *Phys. Rev.* B **60** 7788
[23] Zhao M, Xia Y, Zhang D and Mei L 2003 *Phys. Rev.* B **68** 235415
[24] Zhao M, Xia Y, Tan Z, Liu X, Li F, Huang B, Ji Y and Mei L 2004 *Chem. Phys. Lett.* **389** 160
[25] Durgun E, Tongay S and Ciraci S 2005 *Phys. Rev.* B **72** 075420
[26] Qian Z, Hou S, Zhang J, Li R, Shen Z, Zhao X and Xue Z 2005 *Physica* E **27** 81
[27] Kang J W and Hwang H J 2004 *Comput. Mater. Sci* **31** 237
[28] Saunders V R, Dovesi R, Roetti C, Orlando R, Zicovich-Wilson C M, Harrison N M, Doll K, Civalleri B, Bush I J, D'Arco Ph and Llunell M 2003 *CRYSTAL-03 User Manual* University of Turin
[29] Perdew J P and Wang Y 1986 *Phys. Rev.* B **33** 8800
Perdew J P and Wang Y 1989 *Phys. Rev.* B **40** 3399
Perdew J P and Wang Y 1992 *Phys. Rev.* B **45** 13244
[30] Catti M, Valerio G, Dovesi R and Causá M 1994 *Phys. Rev.* B **49** 14179
[31] Gulans A, Evarestov R A, Tale I and Yang C C 2005 *Phys. Status Solidi* c **2** 507
[32] Monkhorst H J and Pack J D 1976 *Phys. Rev.* B **13** 5188
[33] Gilat G 1982 *Phys. Rev.* B **26** 2243
[34] Litimein F, Bouhafs B, Dridi Z and Ruterana P 2002 *New J. Phys.* **4** 64